Dynamic response of micropipettes during piezo-assisted intracytoplasmic sperm injection

Mehdi Karzar-Jeddi, Nejat Olgac, and Tai-Hsi Fan*
Department of Mechanical Engineering, University of Connecticut, Storrs, Connecticut 06269-3139, USA
(Received 21 July 2011; published 7 October 2011)

In the intracytoplasmic sperm injection (ICSI) process, a piezoelectric actuator is commonly used to assist the piercing of cell membrane. The longitudinal pulses that are performed by the piezo actuator, however, cause undesired lateral vibrations at the drawn tip of the injection micropipette. This mechanism is not well understood, despite its critical role in piezo-assisted cellular microinjection. We provide an analytical model to characterize the micropipette tip vibrations under assumed base excitation arising from the piezoelectric pulses. The resulting dynamic response is determined by using the Duhamel integral method. This study quantifies the effect of fluid damping, embedded mercury, and the apparent cell membrane elasticity. We found that, in practice, a small mercury droplet filled in pipette essentially creates higher shear forces at the membrane-pipette interface. The increased shear due to underdamped eigenmodes is conceived to assist the piercing of the cell membrane.

DOI: 10.1103/PhysRevE.84.041908 PACS number(s): 87.80.Fe, 43.40.+s, 46.40.−f, 87.16.D−

I. INTRODUCTION

Microinjection is a well-accepted method to introduce sperm, nucleus, DNA materials, or macromolecules into biological cells for biomedical research and applications such as infertility treatment, cloning, and cryopreservation [1–3]. The procedure starts with penetration of a glass micropipette through the cytoplasmic membrane followed by substance delivery into the cells. Here we focus on the intracytoplasmic sperm injection (ICSI) process, which is one of the broadly used fertilization techniques. During ICSI the oocyte (unfertilized egg) is immobilized by a holding pipette, and then an injection pipette penetrates through both the zona pellucida and oolemma to introduce the sperm into the oocyte's cytoplasm [4,5]. The zona pellucida is a polymer layer made of glycoproteins that enclose the whole oocyte [6], whereas the oolemma is the cytoplasmic membrane. Piercing through the oolemma of a mouse oocyte is difficult due to its high flexibility and compliance to the motion of the injection pipette. To assist the penetration, a piezo-driven longitudinal pulse train is commonly introduced to the injecting pipette (Fig. 1). However, this pulse train unavoidably excites lateral vibrations at the pipette holder and the micropipette [7]. It is believed that the lateral vibration at the pipette-membrane contact point may damage the oolemma and thus reduce the success rate of ICSI. In practice today, this difficulty is overcome by filling the pipette tip with mercury. However, there is no supporting comprehensive analysis to this claim. Contradicting viewpoints also exist on whether fluid damping can significantly suppress the tip vibration prior to and during the oocyte penetration process [7–9]. Furthermore, it is not clear whether the lateral vibration in such a short period of time (usually around milliseconds) assists the membrane penetration or yields harmful effects to the oocyte. This study provides an analysis to clarify the added mercury, fluid damping, and piezo-triggered tip vibration effects from the continuum-mechanics viewpoint.

Dynamic response of the micropipette can be modelled as a Euler-Bernoulli beam with a fluid damping effect. Such mathematical framework is similar to those used for simulating resonant behaviors of an atomic force microscope (AFM) cantilever tip driven by a harmonic base motion [10–12]. For a very small oscillation amplitude compared to the beam thickness or pipette diameter, the fluid damping force acting on the cantilever can be approximated by using the classical boundary layer theory [13]. For a simple cylindrical cantilever beam the linear streaming model can be solved analytically. A finite element numerical analysis of the dynamic response of the micropipette under oscillatory forcing was provided by Fan *et al.* [9]. However, the boundary layer model is applicable for small-amplitude oscillation and not appropriate for characterizing the fluid damping effect caused by the large-amplitude oscillations of the ICSI micropipette, which was clearly observed from the optical images provided by Ediz and Olgac [7,8]. In principle, the distinct flow pattern induced by large-amplitude pipette oscillation can be resolved only numerically. To simplify the model, here we use an empirical approximation of the drag force on an oscillating cylinder to quantify the fluid damping effect under the pulse-excited vibration. The indentation resistance from the membrane is modelled by an axial force applied to the pipette, and the shear effect is simplified based on apparent viscoelastic properties of the oolemma cell membrane.

II. ANALYSIS

The assembly for piezo-assisted ICSI consists of three major components: piezoelectric actuator, pipette holder, and glass pipette that is drawn to a very narrow tip with diameter around 10 μm (Fig. 1). The actuator generates an axial pulse train that leads to an apparent decaying lateral vibration near the pipette holder. Direct measurement of the pipette vibration is very difficult; however, the excited lateral vibration was successfully detected by a noncontact photonic probe at the pipette holder [8], showing that a 2-Hz longitudinal pulse train given by the piezoelectric actuator excites about 6-kHz lateral decaying vibration with duration about 4 ms. The majority of the micropipette can be assumed solid except the drawn tip. Thus, one can assume that the lateral vibration at the pipette holder is transmitted up to the narrowing shoulder without attenuation. This base vibration subsequently excites

*Corresponding author: thfan@engr.uconn.edu

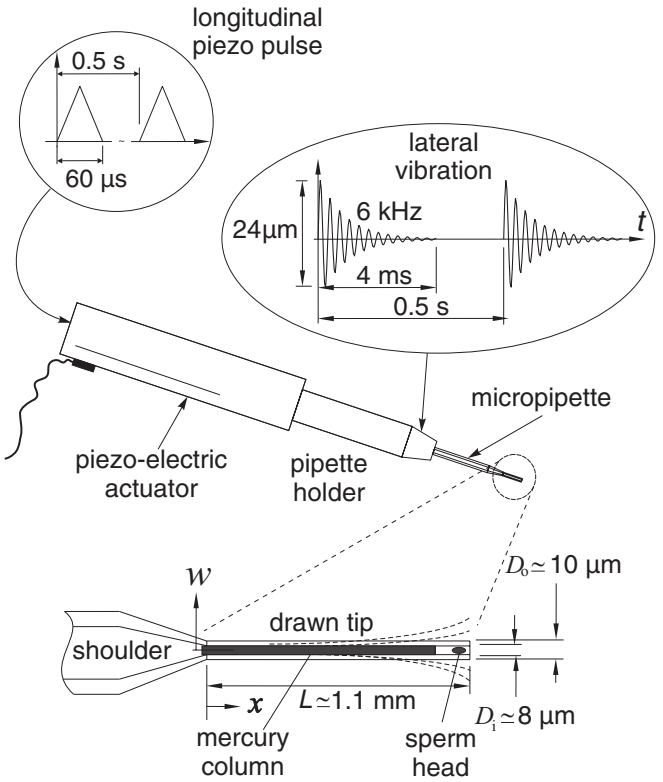

FIG. 1. Schematic of a micropipette assembly. The longitudinal pulse train is introduced by the piezo actuator and is carried through the pipette holder. As a result, the pipette shoulder undergoes a decaying lateral oscillation excited by the longitudinal piezo pulse train. The drawn pipette is filled with the culture medium and mercury before aspiration of the sperm head near the pipette mouth.

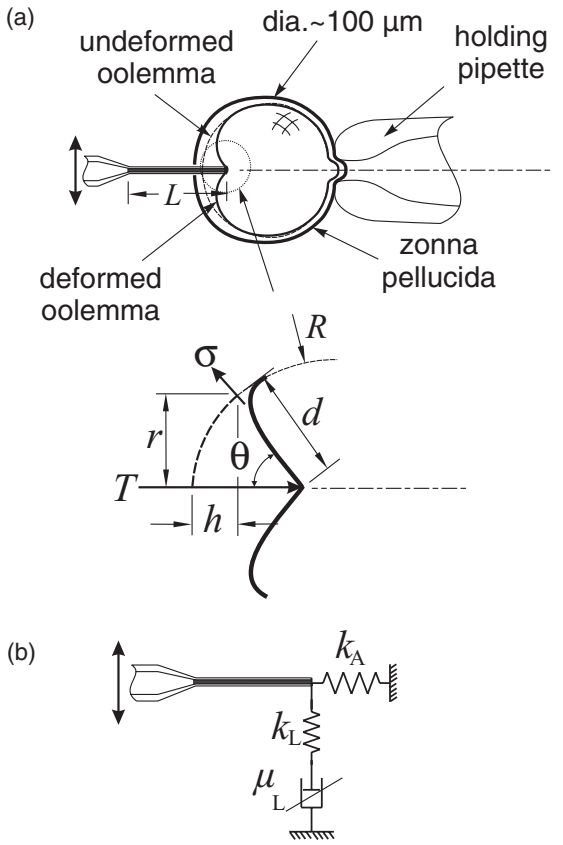

FIG. 2. (a) Axisymmetric schematic of oocyte in contact with the pipette tip and (b) a phenomenological model for the membrane indentation effect.

the flexible pipette tip. In an ICSI procedure the drawn tip is fully immersed in the culture medium with viscosity similar to water. The free vibration of the tip is suppressed by this surrounding medium and additionally by the embedded mercury. Moreover, when the tip indents the oolemma, the lateral and axial forces between the pipette tip and the oolemma membrane should be considered. To facilitate the analysis, a few important assumptions are made: (i) there is no slip between the tip and the membrane, (ii) the structural damping due to the energy dissipation of the glass material and the friction between the glass and mercury is negligible, and (iii) the small pipette section for sperm head deployment is neglected and the drawn pipette tip is assumed either empty or completely filled with mercury (two limiting cases).

A. Mathematical model

Presuming the structure of the vibrating tip follows the Euler-Bernoulli beam theory [14], the membrane indentation can be incorporated and modelled by an axial compressive load, and the hydrodynamic resistance to the tip is represented by a linear damping effect. The one-dimensional governing equation thus can be written as

$$EI\frac{\partial^4 w}{\partial x^4} + T\frac{\partial^2 w}{\partial x^2} + \rho A\frac{\partial^2 w}{\partial t^2} + c\frac{\partial w}{\partial t} = 0 \qquad (1)$$

for $0 \leqslant x \leqslant L$ and $t \geqslant 0$, where $w(x,t)$ is the lateral displacement of the tip, E is Young's modulus, $I = \pi(D_o^4 - D_i^4)/64$ is the area moment of inertia, in which D_o and D_i are outer and inner diameters of the micropipette (Fig. 1), T represents the axial force, ρ is the structure density, $A = \pi(D_o^2 - D_i^2)/4$ is the pipette tip's cross-sectional area, ρA is the effective mass per unit length, and c (kg $m^{-1}s^{-1}$) is the apparent viscous damping coefficient that accounts for the fluid damping effect. If the pipette is filled with mercury, the effective mass of the pipette tip should be modified and account for the mass of glass and mercury. The axial force T in Eq. (1) is the resistance from the indented oolemma, which is calculated from the tension stress due to the stretching of the membrane [Fig. 2(a)].

Before the indentation, the oocyte is spherical with surface area S_0 about $4\pi R^2$, where R is the oocyte radius. The area of the undeformed spherical cap is $S_1 = 2\pi Rh$ while the deformed part of membrane has conical surface with area $S_2 = \pi rd$. Assuming that the stress distribution is uniform and isotropic, in the meridian direction the tensional stress is $\sigma = k_D(S_2 - S_1)/S_0$, where k_D is the membrane area dilation modulus. Now by integrating the tension stress near the folding edge with radius r, the axial force T can be formulated as

$$T = 2\pi r\sigma\cos\theta. \qquad (2)$$

Furthermore, the moving base of the beam is clamped (Fig. 2), and the two boundary conditions are

$$w(0,t) = a_0 e^{-\epsilon t}\sin(2\pi\omega_0 t) \quad \text{and} \quad \frac{\partial w}{\partial x} = 0 \quad \text{at} \quad x = 0, \tag{3}$$

where a_0 is the initial amplitude of vibration, ϵ represents an empirical decaying rate of the forced vibration at the shoulder, and ω_0 is the forcing frequency. These parameters are determined from the measurement using a photonic sensor placed near the pipette holder [7].

Assuming that the point contact between the tip and the membrane has no bending resistance, the bending moment for the tip vanishes and is expressed as

$$\frac{\partial^2 w}{\partial x^2} = 0 \quad \text{at} \quad x = L. \tag{4}$$

Additionally, it was found that lipid bilayer membrane has viscoelastic properties [15,16], and, thus, the membrane response due to the shearing motion from the tip at the contact point may be represented by the Maxwell viscoelastic model [17] with a serial arrangement of a spring and a dashpot [Fig. 2(b)] and expressed as

$$\tau + \frac{\mu_L}{k_L}\frac{\partial \tau}{\partial t} = \mu_L \dot{\gamma} \quad \text{at} \quad x = L, \tag{5}$$

where τ is the shear stress, μ_L is the apparent membrane viscosity, k_L is the membrane modulus, and $\dot{\gamma}$ is strain rate at the contact point. Assuming that there is no slip at the contact point, the above Maxwell boundary condition can be formulated in terms of the tip displacement as

$$EI\frac{\partial^3 w}{\partial x^3} + EI\frac{\mu_L}{k_L}\frac{\partial^4 w}{\partial x^3 \partial t} = \mu_L \frac{\partial w}{\partial t}. \tag{6}$$

The initial conditions for the beam equation [Eq. (1)] are $w(x,0) = \dot{w}(x,0) = 0$.

Considering the following characteristic scales:

$$\begin{aligned} &\text{length} \sim L, \quad \text{displacement} \sim a_0, \\ &\text{time} \sim \omega_0^{-1}, \quad \text{frequency} \sim \omega_0, \end{aligned} \tag{7}$$

where ω_0 ($\simeq$6 kHz) is the driving frequency from the pulse train applied to the micropipette base, the scaled beam equation becomes

$$\lambda\frac{\partial^4 w^*}{\partial x^{*4}} + \zeta\frac{\partial^2 w^*}{\partial x^{*2}} + \frac{\partial^2 w^*}{\partial t^{*2}} + \kappa\frac{\partial w^*}{\partial t^*} = 0, \tag{8}$$

for $0 \leqslant x^* \leqslant 1$ and $t^* \geqslant 0$, where x^* and t^* are scaled spatial and temporal variables, respectively. The corresponding boundary conditions are

$$\begin{aligned} w^*(0,t^*) &= e^{-\eta t^*}\sin(2\pi t^*), \\ \frac{\partial w^*}{\partial x^*}(0,t^*) &= 0, \\ \frac{\partial^2 w^*}{\partial x^{*2}}(1,t^*) &= 0, \\ \psi\frac{\partial^3 w^*}{\partial x^{*3}}(1,t^*) + \frac{\partial^4 w^*}{\partial x^{*3}\partial t^*}(1,t^*) &= \varphi\frac{\partial w^*}{\partial t}(1,t^*). \end{aligned} \tag{9}$$

The dimensionless groups are defined as

$$\begin{aligned} &\lambda = \frac{EI}{\omega_0^2 L^4 \rho A}, \quad \zeta = \frac{T}{\omega_0 L^2 \rho A}, \quad \kappa = \frac{c_0}{\omega_0 \rho A}, \\ &\eta = \frac{\epsilon}{\omega_0}, \quad \psi = \frac{k_L}{\mu_L \omega_0}, \quad \text{and} \quad \varphi = \frac{k_L L^3}{EI}, \end{aligned} \tag{10}$$

which measure the relative contributions of elastic to structure inertial effect (λ), axial load to structural inertial effect (ζ), viscous damping to structure inertial effect (κ), decay rate of the forcing frequency to the forcing frequency (η), the forcing to membrane relaxation time scales (ψ), and the lateral elasticity of membrane to the elasticity of the micropipette beam (φ). Note that λ is equivalent to the stiffness of the beam, and the axial force in ζ provides a compressive effect that reduces the natural frequency of tip vibration. The hydrodynamic viscous damping in κ does not affect the nature of the beam but does determine whether the vibrating modes are overdamped. The membrane relaxation time scale is of the order of 10^{-1} s [15], which is much higher than the tip oscillation time scale ($\sim 10^{-4}$ s). Therefore, ψ is around 10^{-3}, meaning the membrane viscous effect is negligible at this driving frequency, and the Maxwell boundary condition reduces to a simple spring model for the lateral displacement. In dimensionless form, it is

$$\frac{\partial^4 w^*}{\partial x^{*3}\partial t^*}(1,t^*) \simeq \varphi\frac{\partial w^*}{\partial t}(1,t^*). \tag{11}$$

Integrating the above equation with time and considering the zero initial condition, we obtain:

$$\frac{\partial^3 w^*}{\partial x^{*3}}(1,t^*) = \varphi w^*(1,t^*), \tag{12}$$

Other dimensionless groups are of the order of 1 to 10, and, therefore, the corresponding terms are kept in the formulation.

During ICSI the pipette tip is fully immersed in the oocyte culture medium with a viscosity similar to water. As a result, a damping force arises to suppress vibration of the pipette tip. This force is similar to the damping force from viscous fluid to an oscillating cylinder. The fluid flow induced by an oscillating cylinder has complicated patterns, including a streaming boundary layer for small-amplitude oscillation [13] and vortex shedding behind the cylinder. These patterns are characterized by the Reynolds number (Re), the Keulegan-Carpenter number (KC), and/or the Stokes' parameter (β) [18,19]. However, analytical solutions exist only for cases with low-Re and low-KC regime and small oscillation amplitude, so the boundary layer approximation is applicable for finding the frequency response and hydrodynamic resistance of a cantilever beam [9,12]. As mentioned in the Introduction, such an approximation is not appropriate for determining the damping force on the oscillatory micropipette considered for an ICSI application. In our case, for medium density $\sim 10^3$ kg/m^3, viscosity $\sim 10^{-3}$ kg m^{-1}s^{-1}, tip diameter 10 to 22 μm, Re $\sim$ 10 to 30, KC $\sim$ 5 to 50, and $\beta \sim O(1)$, a pair of symmetric vortices may appear behind the cylinder or even detach from the cylinder surface when the moving direction of the cylinder changes [18]. The total drag of the oscillating cylinder is composed of (i) the quasisteady viscous drag and (ii) the force history primarily due to the reversal of the motion

direction [20]. Because the main contribution of the total drag comes from the viscous effect, to facilitate the analytical study, here we consider only the quasisteady approximation for the fluid damping on the dynamic response of the micropipette. A reasonable estimation of such damping can be calculated by the drag coefficient and an estimated linear relation between the local drag force and the moving velocity of the drawn tip. The local drag force per unit length can be calculated by

$$F_D = \varrho U^2 D C_D/2, \tag{13}$$

where ϱ is density of fluid, U is the lateral velocity of micropipette, D is diameter of micropipette, and C_D is the drag coefficient. Without direct numerical simulation of the complicated flow, the drag force can be estimated by the scaling relationship [21]:

$$C_D \simeq 1 + 10\mathrm{Re}_D^{-2/3}, \tag{14}$$

which represents a uniform flow passing through a cylinder with Re ranging from creeping flow regime up to the order of 10^5. For the given fluid density and cylinder diameter, the dimensional local damping force per unit length can be simplified as

$$F_D \simeq 0.0075U^2 + 0.0123U^{4/3}, \tag{15}$$

where

$$U = (a_0\omega_0)\partial w^*/\partial t^*. \tag{16}$$

A reasonable linear approximation of the scaling relationship $F_D \sim cU$ is good for Re up to 30 and the corresponding drag coefficient $c \simeq 0.025$ (kg m^{-1}s^{-1}). Comparing with the reported numerical results [20], this approximation underestimates the damping effect by about 10% due to the neglected force history for a cylinder undergoing a large-amplitude oscillation.

B. Integral solution

The asterisk superscript is dropped hereafter in this section for convenience. The proposed mathematical model includes a time-dependent boundary condition [the first condition in Eq. (9)] and can be solved by the Duhamel integral method [22]. This method is in general applicable for a linear equation with time-dependent nonhomogeneous boundary condition arising from the forcing effect. For this purpose the corresponding auxiliary problem for the dynamic response of the step input has to be solved, expressed as

$$\lambda\frac{\partial^4 u}{\partial x^4} + \zeta\frac{\partial^2 u}{\partial x^2} + \frac{\partial^2 u}{\partial t^2} + \kappa\frac{\partial u}{\partial t} = 0, \tag{17}$$

where u is the solution for the corresponding auxiliary problem and the boundary conditions are $u(0,t) = 1, u'(0,t) = 0, u''(1,t) = 0$, and $u'''(1,t) = \varphi u(1,t)$, and the initial conditions $u(x,0) = 0$ and $\dot{u}(x,0) = 0$ indicate that the micropipette is initially at rest without deformation. The solution for the auxiliary problem is a sum of the steady state and transient solutions, $u(x,t) = f(x) + v(x,t)$. The steady-state part satisfies

$$\frac{\partial^4 f(x)}{\partial x^4} + \frac{\zeta}{\lambda}\frac{\partial^2 f(x)}{\partial x^2} = 0 \tag{18}$$

with boundary conditions $f(0) = 1$, $f'(0) = 0$, $f''(1) = 0$, and $f'''(1) = \varphi f(1)$. The last two conditions describe the spring-hinged conditions. The solution of the steady-state formulation is, therefore,

$$f(x) = A_1\cos(\alpha x) + A_2\sin(\alpha x) + A_3 x + A_4, \tag{19}$$

where the coefficients are

$$\begin{aligned} A_1 &= \frac{\varphi\tan\alpha}{\alpha^3[(\tan\alpha)(\sin\alpha) + \cos\alpha] - \varphi[\alpha - \tan\alpha]}, \\ A_2 &= \frac{-A_1}{\tan\alpha}, \quad A_3 = -\alpha A_2, \quad \text{and} \quad A_4 = 1 - A_1. \end{aligned} \tag{20}$$

Note that $\alpha^2 = \zeta/\lambda$ gives the comparison of the axial force to the pipette tip's stiffness.

The resulting equation for the transient part $v(x,t)$ is formulated as

$$\lambda\frac{\partial^4 v}{\partial x^4} + \zeta\frac{\partial^2 v}{\partial x^2} + \frac{\partial^2 v}{\partial t^2} + \kappa\frac{\partial v}{\partial t} = 0, \tag{21}$$

where the boundary conditions are $v(0,t) = 0$, $v'(0,t) = 0$, $v''(1,t) = 0$, and $v'''(1,t) = \varphi v(1,t)$ and the initial conditions are $v(x,0) = -f(x)$ and $\dot{v}(x,0) = 0$. Letting $v_n(x,t) = X_n(x)T_n(t)$ we obtain the eigenequation:

$$\frac{\partial^4 X(x)}{\partial x^4} + \frac{\zeta}{\lambda}\frac{\partial^2 X(x)}{\partial x^2} - \frac{\omega_{\mathrm{n}}^2}{\lambda}X(x) = 0, \tag{22}$$

where ω_n is the natural frequency. The boundary conditions corresponding to the eigenfunction are $X(0) = 0$, $X'(0) = 0$, $X''(1) = 0$, and $X'''(1) = \varphi X(1)$. The mode shape of the uniform beam $X_n(x)$ can thus be derived and expressed as

$$\begin{aligned} X_n(x) = {} & \cosh(k_{n1}x) - \cos(k_{n2}x) - [\sinh(k_{n1}x) - \sin(k_{n2}x)] \\ & \times \left[\frac{k_{n1}^2\cosh k_{n1} - k_{n2}^2\cos k_{n2}}{k_{n1}^2\sinh k_{n1} - k_{n1}k_{n2}\sin k_{n2}}\right], \end{aligned} \tag{23}$$

where

$$\begin{aligned} k_{n1} &= \left\{2\zeta/\lambda + \left[4(\zeta/\lambda)^2 + k_{\mathrm{n}}^4\right]^{\frac{1}{2}}\right\}^{\frac{1}{2}}, \\ k_{n2} &= \left\{-2\zeta/\lambda + \left[4(\zeta/\lambda)^2 + k_{\mathrm{n}}^4\right]^{\frac{1}{2}}\right\}^{\frac{1}{2}}, \end{aligned} \tag{24}$$

and $k_n = (\omega_n/\lambda)^{\frac{1}{4}}$ is the flexural wave number connected to the natural frequencies ω_n and the stiffness parameter λ. The corresponding frequency equation becomes

$$\begin{aligned} 0 = {} & \left[k_{n1}^2\cosh k_{n1} + k_{n2}^2\cos k_{n2}\right]\left\{k_{n1}^3\cosh k_{n1}\right. \\ & \left. + k_{n1}k_{n2}^2\cos k_{n2} - \varphi\left[\sinh k_{n1} - \frac{k_{n1}}{k_{n2}}\sin k_{n2}\right]\right\} \\ & - \left[k_{n1}^2\sinh k_{n1} + k_{n1}k_{n2}\sin k_{n2}\right]\left\{k_{n1}^3\sinh k_{n1} - k_{n2}^3\sin k_{n2}\right. \\ & \left. - \varphi[\cosh k_{n1} - \cos k_{n2}]\right\}. \end{aligned} \tag{25}$$

The temporal equation is

$$\frac{\partial^2 T}{\partial t^2} + \kappa\frac{\partial T}{\partial t} + \omega_n^2 T = 0 \tag{26}$$

for $\dot{T}(0) = 0$, and the solution is

$$T_n(t) = e^{-\kappa t/2}\left(e^{\beta_n t} + \frac{2\beta_n - \kappa}{2\beta_n + \kappa}e^{-\beta_n t}\right), \tag{27}$$

where β_n is the damped vibration frequency of the micropipette as a a function of dimensionless natural frequency ω_n and the damping factor κ:

$$\beta_n = \left[(\kappa/2)^2 - \omega_n^2\right]^{1/2}. \tag{28}$$

From the initial condition $v(x,0) = -f(x)$, the following solution for the auxiliary problem can be obtained:

$$u(x,t) = f(x) - \sum_{n=1}^{\infty} \frac{(2\beta_n + \kappa)\int_0^1 f(x)X_n dx}{4\beta_n \int_0^1 X_n^2 dx} T_n(t)X_n(x). \tag{29}$$

The summation is the time-dependent contribution of every eigenmode. Finally, based on the Duhamel integral method, the complete vibration can be expressed as a closed form integral solution:

$$w(x,t) = \int_0^t u(x,t-\tau)\frac{\partial w}{\partial t}(0,\tau)d\tau, \tag{30}$$

where u is the response of the micropipette to a unit step input at the base ($x = 0$) and $\partial w(0,\tau)/\partial t$ represents the velocity of the lateral motion at the base.

III. RESULTS AND DISCUSSION

A. A free-vibrating tip

The dynamic features of the micropipette can be understood from a free-vibrating tip ($\zeta = 0, \varphi = 0$), which is governed by the damped Euler-Bernoulli beam equation. For this special case, the eigenmode reduces to

$$X_n(x) = \cosh(k_n x) - \cos(k_n x) - \frac{\cosh(k_n) + \cos(k_n)}{\sinh(k_n) + \sin(k_n)}[\sinh(k_n x) - \sin(k_n x)], \tag{31}$$

and the corresponding characteristic equation is

$$1 + \cos k_n \cosh k_n = 0, \tag{32}$$

which yields the wave numbers (k_n) 1.875, 4.694, 7.854, 10.99, and so on. The transient solution is the same as Eq. (27). Therefore,

$$u(x,t) = 1 - \sum_{n=1}^{\infty} \frac{(2\beta_n + \kappa)\int_0^1 X_n dx}{4\beta_n \int_0^1 X_n^2 dx} T_n(t)X_n(x), \tag{33}$$

and $w(x,t)$ again can be found by Eq. (30). As a result, we calculate the tip response to a continuous input function $w(0,t) = a_0 \tanh(\tau_0 t)$ that represents the impulse. The parameters corresponding to the experimental setting are as follows: $L = 1.1$ mm, $\rho_{\text{glass}} = 2{,}290$ kg/m^3, $\rho_{\text{Hg}} = 13\,543$ kg/m^3, $E = 63.4$ GPa, $A_{\text{glass}} = 2.827 \times 10^{-11}$ m^2, $A_{\text{Hg}} = 5.027 \times 10^{-11}$ m^2, $I = 2.898 \times 10^{-22}$ m^4, $\omega_0 = 6$ kHz, empirical decaying rate $\gamma = 1000$ s^{-1}, initial amplitude $a_0 = 12$ μm, and τ_0 is set to 100 s^{-1} for a short duration of the step. The dynamic response of micropipette tip in fluid to this input is illustrated for cases of empty micropipette and pipette filled with mercury.

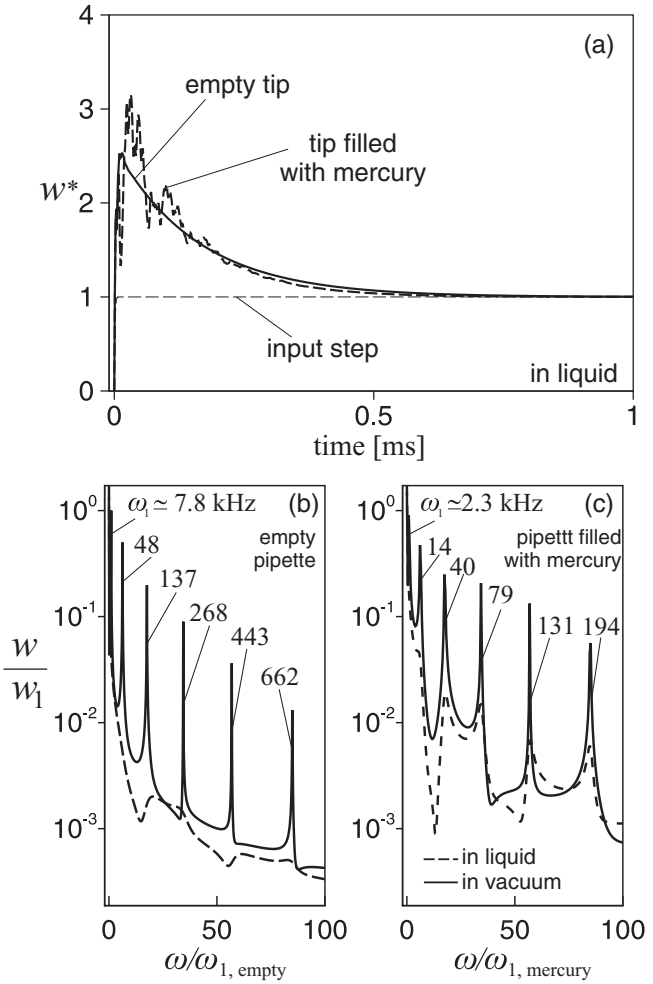

FIG. 3. Dynamic response at the free end of the drawn pipette tip to a step input in liquid: (a) the beam deflection w^* (scaled by $a_0 = 12$ μm) for an empty drawn pipette tip and a tip filled with mercury; (b) dynamic response in the frequency domain for an empty tip ($\lambda = 5.38$ and $\kappa = 64.4$, w is scaled by the first eigenmode contribution, amplitude w_1); and (c) response for a tip filled with mercury ($\lambda = 0.47$, $\kappa = 5.59$).

In Fig. 3(a), the step response for the micropipette tip immersed in viscous fluid shows that the triggered oscillation has an overshoot regardless the existence of mercury. After the initial overshoot, the vibration damps out quickly to a new position $w^* = 1$ with almost the same settling time for both cases. For empty micropipette the damping profile is smooth. For the pipette filled with mercury the average damping and settling time are almost the same as the empty pipette, whereas the contributions of higher harmonics cause significant noise. Figures 3(b) and 3(c) show the dynamic response at the end of the tip in the frequency domain, both in vacuum and immersed in a viscous fluid. All lateral deflections are rescaled by $w_1 \simeq 17.4$ μm, which is the amplitude of the first eigenmode of the empty micropipette in vacuum. The frequencies are scaled by the first natural frequency corresponding to the empty tip and to the tip filled with mercury. In Fig. 3(b), for an empty pipette the fluid damping effect suppresses all of the eigenmode contributions, while Fig. 3(c) shows

that for the pipette filled with mercury the contribution from higher eigenmodes is still quite effective under fluid damping. Comparing Figs. 3(b) and 3(c), the mercury case contributes more to the lateral vibration for higher eigenmodes, either with or without fluid damping. Therefore, the high frequency oscillation observed in Fig. 3(a) (shown by the dashed line) is the result of higher amplitudes and at higher eigenmodes.

Figure 4 shows the mercury effect on the response of the micropipette under decaying base oscillation without fluid damping. The dimensionless groups $\kappa = 0$, $\eta = 0.17$, and $\lambda = 5.38$ are used for the empty micropipette and $\lambda = 0.47$ is used for the tip filled with mercury. Recall that the λ value measures the relative contribution of structure elasticity to the inertia effect of drawn tip. For large λ the oscillation amplitude near the free end is significantly larger, whereas with the mercury the high inertia reduces the beam stiffness and results in a lower vibration amplitude, and thus the deflection of the whole tip levels off significantly. This result is qualitatively consistent with experimental observations (Figs. 9 and 10 in Ref. [7]), showing that the added mercury reduces the amplitude at the end of the tip by two- to fivefold [Figs. 4(a) to 4(c)]. Figures 4(d) and 4(e) show the dynamic response at the tip end to the decaying forced vibration at the base. In Fig. 4(d) for an empty tip, the first natural frequency ω_1 is very close to the forcing frequency ω_0. This causes larger amplification of the amplitude. However, for the tip filled with mercury [Fig. 4(e)], natural frequencies are away from ω_0 which leads to a smaller amplitude response. The first mode for an empty tip has about fourfold higher amplitude than the tip filled with mercury. This is consistent with the beam shapes observed in Figs. 4(a) and 4(b).

By adding the hydrodynamic damping effect (i.e., pipette in liquid), one observes a reduction of the lateral vibration especially for an empty tip (shown in Fig. 5). Overall, the fluid damping is more efficient for an empty tip with lower inertia and a higher κ value. This agrees well with the complete tip response to the base excitation Eq. (3) that is shown in Fig. 3. With fluid damping, the tip vibration behaves surprisingly similarly for cases with and without embedded mercury. Note that this observation is contingent on the parametric selection for the pipette and the ambient medium. Variations of these parameters can easily reverse the comparative outlook. It is safe to state, however, that the mercury-filled pipette has fewer oscillations in the biological liquid medium than in the air. This is an intuitively obvious result.

The highlight finding of this paper, on the other hand, is as followings. The authors of Ref. [7] compare the pipette tip responses between the empty tip and tip filled with mercury cases while they are in the air. They declare from this observation that the similar comparison should hold when the pipette is in the liquid. The present study brings a contrary viewpoint, whereby induction of a properly selected viscous damping for the medium could render almost identical tip movements for the two pipettes (with and without mercury) in the viscus liquid medium. We may even state that the ambient liquid can be selected such that the earlier proposed advantage of having mercury in the pipette could be, in fact, a handicap. This is a very sensitive point that has not been recognized in earlier investigations.

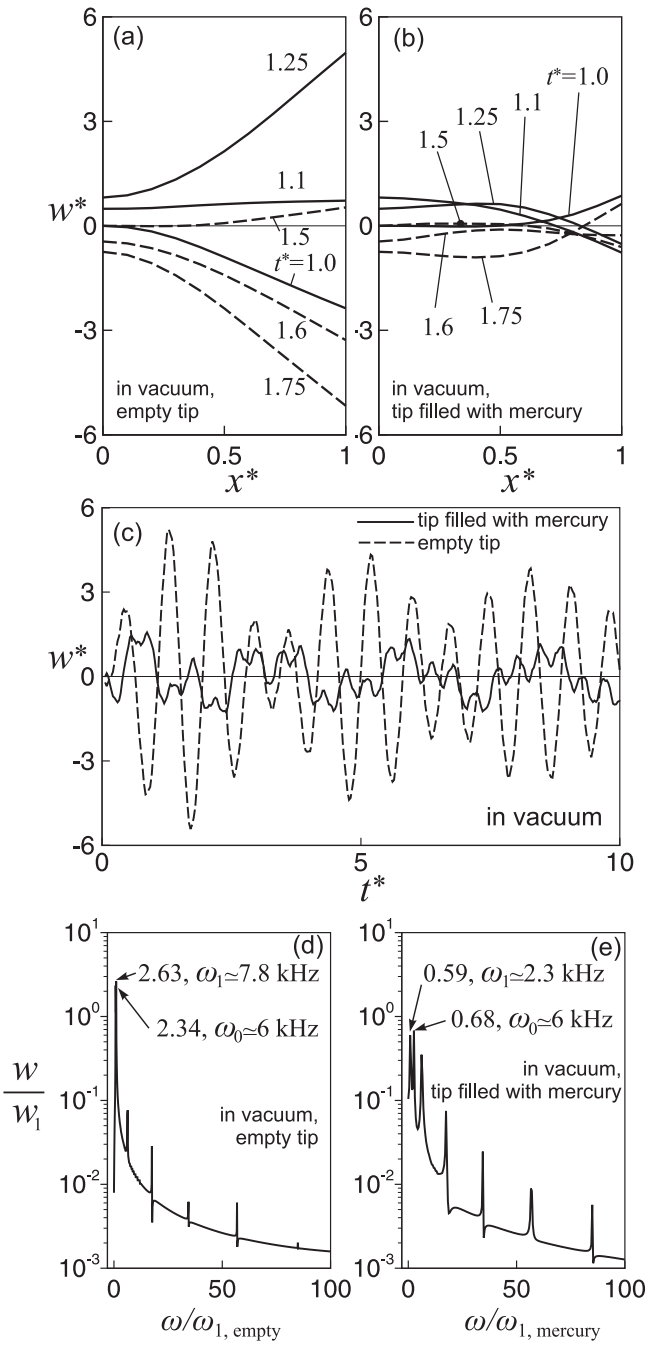

FIG. 4. Response to the base excitation of a drawn tip without the fluid damping effect: (a) the transient beam profiles for an empty drawn tip at a range of dimensionless time $t^* = 1$ to 1.75 ($t^* = \omega_0 t$, $1/\omega_0 \simeq 0.17$ ms), which covers the second cycle of the vibration; (b) beam profiles for a tip filled with mercury; (c) time evolution at the tip end for both cases; (d) dynamic response in the frequency domain for an empty tip; and (e) a tip filled with mercury. The location x is scaled by the tip length 1.1 mm, and the lateral deflection w is scaled by the initial amplitude of the forced vibration, 12 μm.

B. Tip in contact with membrane

In this section we add another new and untreated feature of microinjection operation. When the drawn tip is engaged with the oolemma membrane, the membrane generates an axial

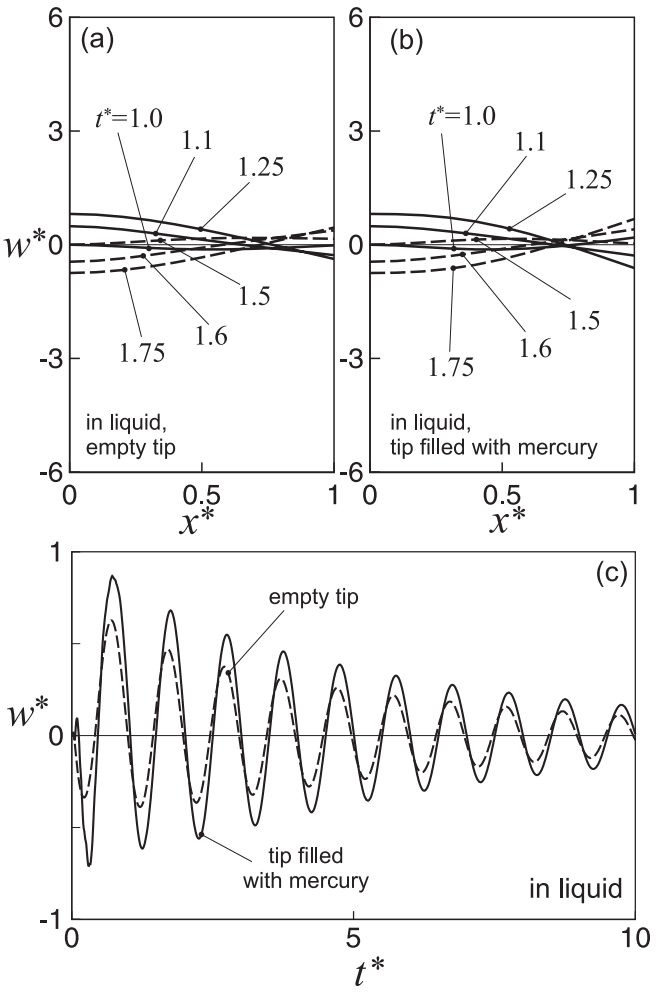

FIG. 5. Fluid damping effect corresponding to the cases presented in Fig. 4. The new dimensionless parameters are as follows: (a) $\lambda = 5.38$, $\kappa = 64.4$, and $\eta = 0.17$ for an empty tip with $\omega_n^* = 7.8$, 48.7, 137.7, and so on; (b) $\lambda = 0.47$, $\kappa = 5.59$, and $\eta = 0.17$ for a tip filled with mercury and $\omega_n^* = 2.3$, 14.4, 40.3, etc.; and (c) the time evolution at the tip end for both cases. Note that for the empty pipette the first mode is overdamped and the higher harmonics are underdamped ($\omega_1^* < \kappa/2 < \omega_2^*, \omega_3^*, \ldots, \omega_\infty^*$), while for the mercury-filled tip all modes are underdamped.

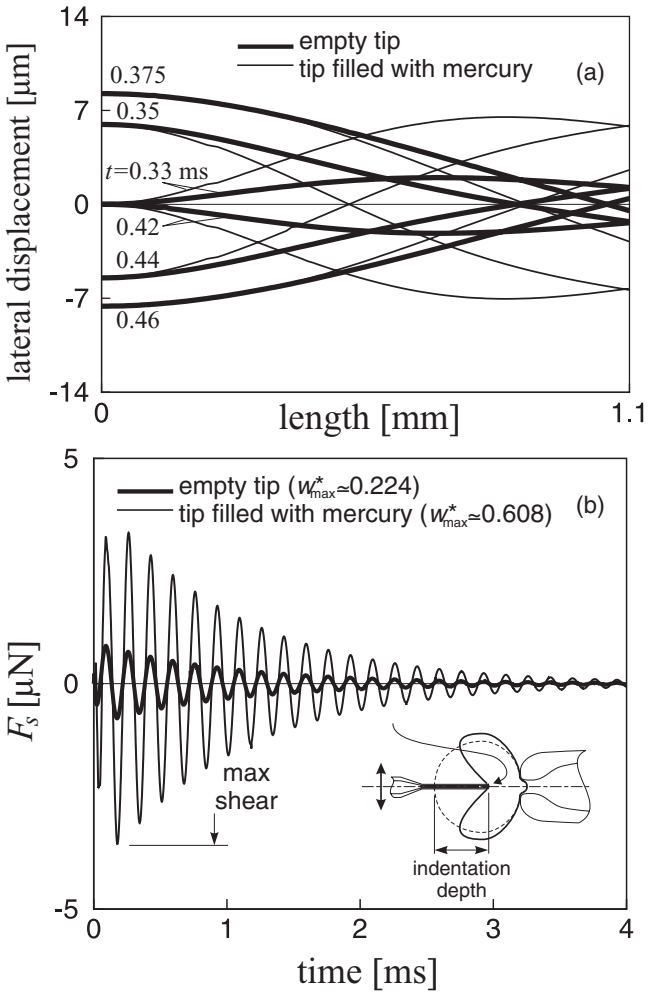

FIG. 6. Pipette engaged in oocyte, all in liquid medium. (a) Transient deflections of the tip at different instants and (b) the estimated shear force acting on the oolemma with and without the mercury. The parameters used are as follows: $\lambda = 5.38$, $\zeta = 1.204$, $\kappa = 64.40$, $\eta = 0.17$, and $\varphi = 32.6$ for an empty tip and $\lambda = 0.47$, $\zeta = 0.07$, $\kappa = 5.59$, $\eta = 0.17$, and $\varphi = 32.6$ for a tip filled with mercury. The indentation depth is around 65% of the oocyte diameter.

force on the tip. This force can be calculated by using Eq. (2). The initial and deformed profiles of the oolemma membrane are measured from optical images [23], and, thus, the axial force T applied to the tip can be calculated. For this purpose, we multiply the relative change of the area, $(S_2 - S_1)/S_0$, with the area dilation modulus k_D (for which a reference value about 450 mN/m [24] is selected) so the tension stress of the membrane σ can be determined. The resulting shear force at the tip-oolemma contact point can also be estimated by $k_L \simeq k_D$ and $F_s = k_D a_0 w^*$ at $x = 1.1$ mm, where w^* is given by the integral solution Eq. (30).

Figure 6 shows the transient shear force applied from the tip to the oolemma. A high shear up to several micronewtons appears during the first few milliseconds. This finding indicates that filling the tip with mercury yields approximately fourfold higher shear force on the oolemma in comparison with the empty tip. This is due to increased inertial effect and the greater contribution from higher harmonics. When filled with mercury the tip displacement at the contact point as well as the applied shear force are much larger. This property possibly eases the piercing the flexible oolemma. According to the frequency response shown in Fig. 3, the higher harmonic vibration of the tip with mercury will provide additional shear to the membrane compared with the empty tip. However, to the best of our knowledge, no experimental evidence or study has ever addressed this issue before.

A few sensitivity tests are presented next in a broader range of membrane stiffness, medium viscous damping, pipette tip length, and the pipette indentation depth on the maximum shear force $F_{s,\max}$. Figure 7(a) shows that a larger membrane elasticity implies a larger shear force when everything else remains the same. In this limit, the shear force vanishes and no resistance exists against the lateral movement of the pipette tip as the membrane elasticity approaches zero. In the other limiting condition for a very stiff membrane, the pipette tip

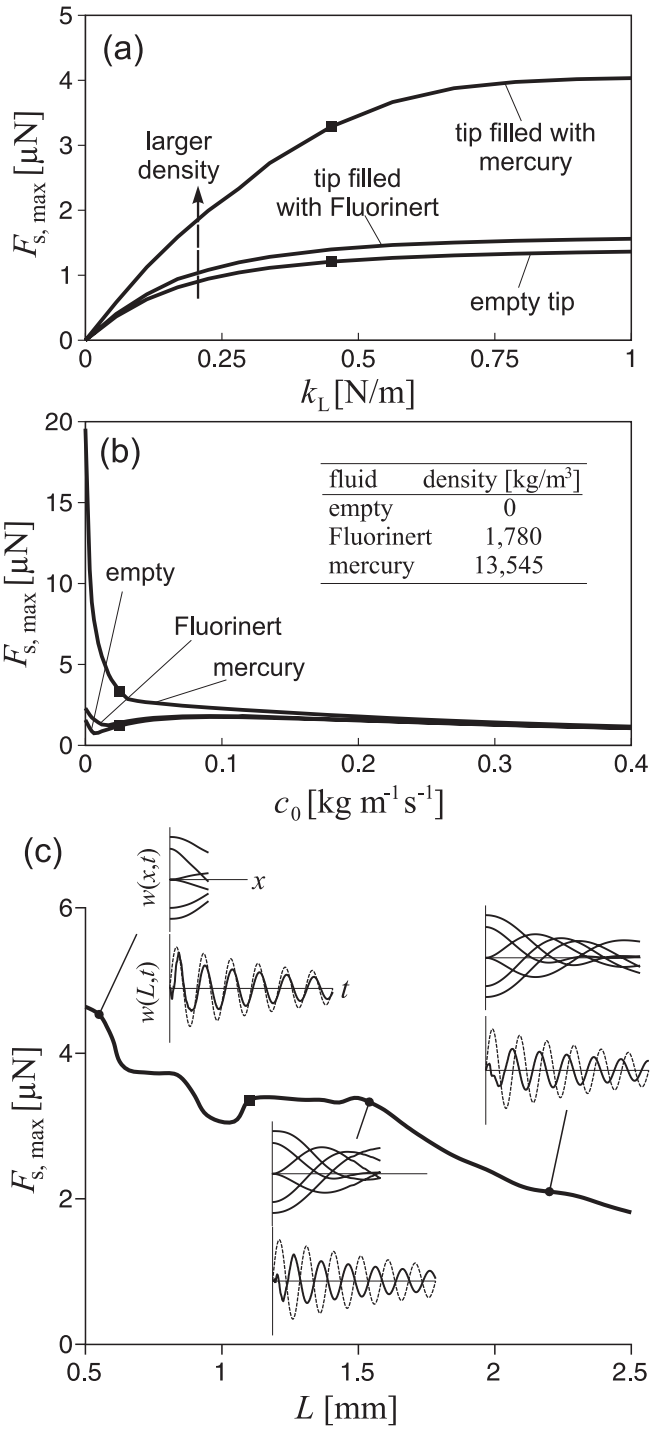

FIG. 7. (a) Effect of membrane elasticity on the maximum shear force while the pipette is in a viscous liquid, (b) viscous damping on the maximum shear force, and (c) pipette tip length on the maximum shear force for the tip filled with mercury; the dashed lines indicate forcing. Squares are data points corresponding to the conditions provided in Fig. 6. The parameters used are as follows: $L = 1.1$ mm, $D_o = 10\,\mu$m, $D_i = 8\,\mu$m, $c = 0.025$ kg ms^{-1}, $\epsilon = 1000$ s^{-1}, $\omega_0 = 6$ kHz, and $a_0 = 1.2\,\mu$m.

is essentially pinned, so $w(L,t) = 0$ and $\partial^2 w(L,0)/\partial x^2 = 0$. This asymptotic behavior yields higher shear forces for all three different filling liquids as shown in Fig. 7(a). Figure 7(b) shows the medium viscous effect on the maximum shear force while all other parameters remain fixed. For the mercury-filled tip, the shear force decreases much more steeply with increasing viscosity and approaches a similar asymptotic value as for the other tips. The shear force monotonically decays as the viscosity increases. In comparison with the less dense filling liquid, such as Fluorinert [5], the tip filled with mercury has the first natural frequency that is much closer to the pulse train frequency at the base (6 kHz). As a result, a resonant response is expected at the tip, which yields a larger amplitude and larger shear force as observed in Fig. 7(b). When the tip is filled with lighter material the medium viscosity does not seem to affect the maximum shear force significantly. All cases approach the limit with a large viscous effect. The effect of the tip length on the maximum shear force is shown in Fig. 7(c). For a short tip the rigidity λ is large enough to keep a relatively flat pipette profile during the vibration and thus the shear force is higher and the trace for the tip end has almost no phase shift compared with the excitation. Applying a longer tip will reduce the rigidity, lead to flexible tip profiles, and cause larger delays in the trace with respect to forcing. Figure 7(c) shows that the shear force does not monotonically decrease as the length increases due to the complicated tip vibration profiles. Multiple inflections along the beam profiles appear for longer tips that may generate a smaller vibration amplitude at the tip end and, thus, smaller maximum shear force. We also expect that longer pipette tips yield higher viscous dissipation effects that limit the vibration amplitude at the tip.

Figure 8 presents the effect of membrane indentation depth on the shear force. A deeper indentation to the oolemma membrane yields a larger axial resistance T to the tip. The resulting maximum shear force $F_{s,max}$ is calculated based on the oolemma profiles [23] at various indentation depths. This earlier study shows that for an indentation depth ranging between 0 and 66% of the oocyte diameter ($\simeq$100 μm), r is around 0 to 37.1 μm, d is about 0 to 63 μm, h is about 0 to 3 μm, and θ is approximately 90° to 30°. The resulting axial force T goes from 0 to approximately 3.96 μN. This value is within the same order of magnitude as that reported by Sun *et al.* [25] and Sen *et al.* [26]. Figure 8 reveals that the maximum shear force remains almost constant for small indentation depth up

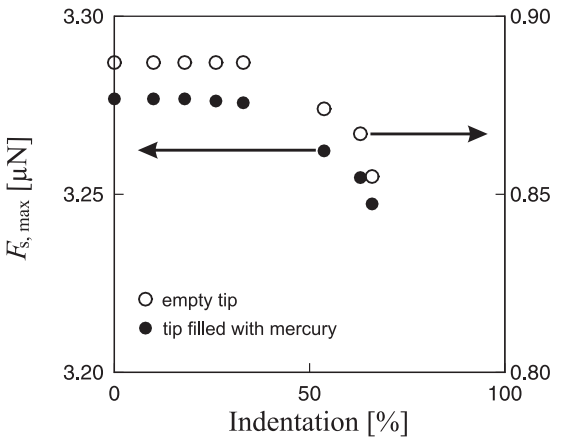

FIG. 8. Effect of indentation depth to the maximum shear force. The parameters are listed in Fig. 7. Note that different scales are applied for different tips.

to 35%. The relative change of the maximum shear force is less than 1% for the tip filled with mercury and ∼3.5% for an empty tip. This shows that the axial load has slight effect on the tip-membrane shear force. Although this percentage seems small, in practice, larger indentation depths may prevent the slip between the tip and the membrane during the lateral vibration of the tip. Because the oolemma's rupture tension is unknown, as a reference, the reported lipid membrane's rupture tension on the order of 10^{-2} N m^{-1} [27,28] is used as a reference. Considering the pipette tip diameter of about 10 μm, the shear force for rupturing membrane is around 0.1 μN. This value is an order of magnitude lower than the shear force shown in Figs. 6 and 8, implying that the oolemma might be pierced by the shear force triggered by the lateral pulse trains instead of the axial piezo-actuated force.

IV. CONCLUSION

This study presents an analysis of piezo-induced tip vibration of an ICSI pipette. The results show that the first few eigenmodes play a major role in the dynamic response of the vibrating tip. Cases with and without embedded mercury in the micropipette are studied in vacuum and in a viscous fluid medium. For selected parametric quantities we observe an interesting comparison: In viscous liquid the pipette tip filled with mercury shows larger strokes than that of the empty pipette. This finding contradicts the current hypothesis among the ICSI community that believes that when the tip is filled with mercury, the movement of the tip is constrained. The mercury-induced larger strokes could cause larger shear force and may ultimately lead to piercing of the cell membrane. The study sheds some light onto this intriguing dynamics. The authors hope that this work will promote further studies and experimental evidence that will bring more engineering tools to the use of practitioners of ICSI.

ACKNOWLEDGMENT

This work is supported by NSF CBET-0828733 and NIH R24RR018934-01.

[1] D. J. Carroll, *Microinjection Methods and Applications* (Humana Press, New York, 2009).
[2] G. Palermo, H. Joris, P. Devroey, and A. C. Van Steirteghem, Lancet **340**, 17 (1992).
[3] P. Devroey and A. Van Steirteghem, Hum. Reprod. Update **10**, 19 (2004).
[4] Y. Kimura and R. Yanagimachi, Biol. Reprod. **52**, 709 (1995).
[5] N. Yoshida and A. CF. Perry, Nat. Protoc. **2**, 296 (2007).
[6] D. P. L. Green, Rev. Reprod. **2**, 147 (1997).
[7] K. Ediz and N. Olgac, J. Biomech. Eng. **127**, 531 (2005).
[8] K. Ediz and N. Olgac, IEEE Trans. Biomed. Eng. **51**(7), 1262 (2004).
[9] M. Fan, Z. C. Feng, Y. Agca, and J. K. Critser, J. Appl. Phys. **100**, 074701 (2006).
[10] D. W. Dareing, T. Thundat, S. Jeon, and M. Nicholson, J. Appl. Phys. **97**, 084902 (2005).
[11] S. Kirstein, M. Mertesdorf, and M. Schönhoff, J. Appl. Phys. **84**, 1782 (1998).
[12] J. E. Sader, J. Appl. Phys. **84**, 64 (1998).
[13] L. Rosenhead, *Laminar Boundary Layers* (Dover, New York, 1988).
[14] S. P. Timoshenko, D. H. Young, and W. Weaver Jr., *Vibration Problems in Engineering* (John Wiley & Sons, New York, 1974).
[15] C. W. Harland, M. J. Bradley, and R. Parthasarathy, Proc. Natl. Acad. Sci. USA **107**, 19146 (2010).
[16] G. E. Crawford and J. C. Earnshaw, Biophys. J. **52**, 87 (1987).
[17] R. B. Bird, R. C. Armstrong, and O. Hassager, *Dynamics of Polymeric Liquids: Fluid Mechanics*, Vol. I. (John Wiley & Sons, New York, 1977).
[18] M. Tatsuno and P. W. Bearman, J. Fluid Mech. **211**, 157 (1990).
[19] B. Uzunoğlu, M. Tan, and W. G. Price, Int. J. Numer. Meth. Eng. **50**, 2317 (2001).
[20] J. R. Chaplin, J. Fluid Mech. **393**, 99 (1999).
[21] F. M. White, *Viscous Fluid Flow* (McGraw-Hill, New York, 1991).
[22] G. E. Myers, *Analyitical Methods in Conduction Heat Transfer* (McGraw-Hill, New York, 1971).
[23] J. F. Diaz, M. Karzar-Jeddi, N. Olgac, T.-H. Fan, and A. F. Ergenc, J. Biomech. Eng. **132**, 121002 (2010).
[24] E. Evans and R. Waugh, Biophys. J. **20**, 307 (1977).
[25] Y. Sun, K.-T. Wan, K. P. Roberts, J. C. Bischof, and B. J. Nelson, IEEE T. Nanobiosci. **2**, 279 (2003).
[26] S. Sen, S. Subramanian, and D. E. Discher, Biophys. J. **89**, 3203 (2005).
[27] E. Evans and W. Rawicz, Phys. Rev. Lett. **79**, 2379 (1997).
[28] D. Needham and R. S. Nunn, Biophys. J. **58**, 997 (1990).